

# Coherent Modulation of Propagating Plasmons in Silver-Nanowire-Based Structures

Zhipeng Li, Shunping Zhang, Naomi J. Halas, Peter Nordlander,\* and Hongxing Xu\*

Silver nanowires with cross sections well below the free-space diffraction limit of light are high-quality waveguides for the propagation of planar, optical-frequency signals as surface plasmon polaritons (SPPs).<sup>[1]</sup> They are currently of intense, rapidly increasing interest as fundamental building blocks of subwavelength optics and as a platform for the development of nanoscale optical components and devices.<sup>[2–12]</sup> A remarkably wide range of plasmonic optical components and devices have been recently demonstrated, including waveguides,<sup>[13–16]</sup> splitters,<sup>[17–19]</sup> routers and multiplexers,<sup>[19]</sup> detectors,<sup>[20,21]</sup> and polarization rotators.<sup>[16,22,23]</sup>

While surface-plasmon modulators have been demonstrated for spatially extended plasmons on metallic films, this highly useful device functionality has not yet been reported for the far more compact nanowire geometry.<sup>[24–26]</sup> Ultimately, nanowire-based modulators could provide a useful functional route to advanced nanoscale analog devices that could operate at optical frequencies.

In this Communication, we demonstrate an interference-based, nanowire all-optical modulator. The device consists of two nanowires: a short nanowire with one of its ends directly adjacent to a main or “trunk” nanowire of longer length, forming a “y” structure. The two adjacent arms of the structure serve as input terminals, with the remaining end of the longer wire as the output. By changing the relative phase or the relative polarization angle of the two input signals, constructive and destructive interference of the plasmons launched onto the main wire occurs, resulting in a strongly modulated emission of the signal at the output. The device functions as a simple nanoscale plasmon modulator, which

could be straightforwardly coupled to other plasmonic components<sup>[16,18,19,27]</sup> in future integrated plasmonic circuits.

The experimental geometry is shown in **Figure 1**. Figure 1a shows a schematic of the optical excitation/modulation/probe geometry. Ag nanowires<sup>[28]</sup> were chemically synthesized and then deposited on an indium tin oxide (ITO)-coated glass substrate where the branched geometries were formed by self-assembly. The transmitted (*EXT 1*) and reflected (*EXT 2*) beams derived from a 633-nm laser source, split by beam-splitter 1 (BS1) so that optics could be inserted

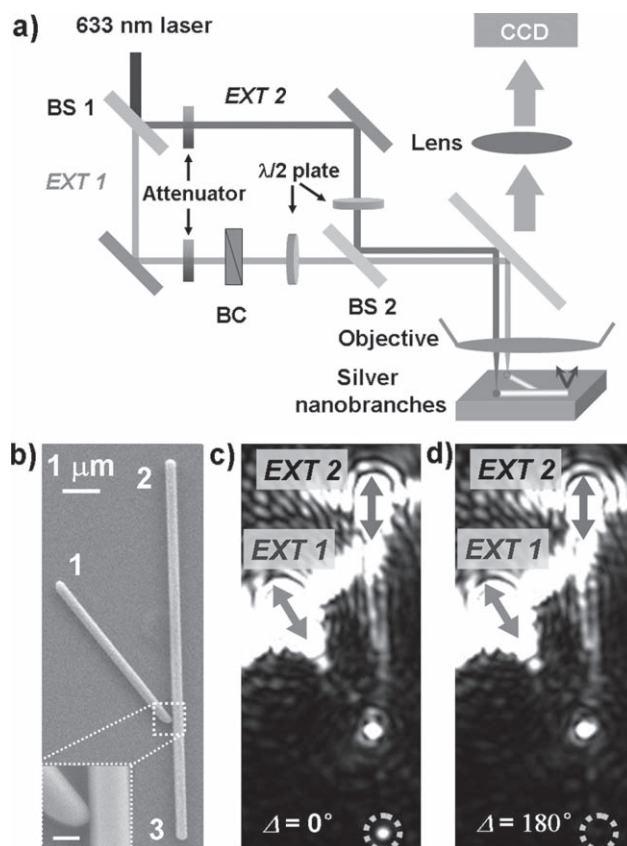


**Figure 1.** A branched nanowire structure as plasmon modulator. a) Experimental setup. Light is split at BS1 into transmitted (*EXT 1*) and reflected (*EXT 2*) beams, recombined at BS2, then focused onto the input sites of the modulator. b) An SEM image of the “y” geometry of the modulator, showing inputs 1 and 2 and output 3. Inset: enlarged view of the junction with the scale bar = 200 nm. c, d) Optical images of the branch excited by two coherent 633-nm laser spots at inputs 1 and 2, respectively. The phase difference of the two SPPs at output 3 are  $\Delta = 0^\circ$  and  $180^\circ$ , for (c) and (d), respectively. Arrows indicate the angle of incident polarization at each input.

Dr. Z. P. Li, S. P. Zhang, Prof. N. J. Halas, Prof. P. Nordlander, Prof. H. X. Xu  
Beijing National Laboratory for Condensed Matter Physics  
Institute of Physics  
Chinese Academy of Sciences  
Box 603–146, 100190, Beijing, China  
E-mail: nordland@rice.edu; hxu@aphy.iphy.ac.cn

Prof. N. J. Halas, Prof. P. Nordlander  
Department of Physics and Astronomy  
Department of Electrical and Computer Engineering  
Laboratory for Nanophotonics  
Rice University  
Houston, TX 77005, USA

Prof. H. X. Xu  
Division of Solid State Physics/The Nanometer Consortium  
Lund University  
Box 118, S-22100, Lund, Sweden

DOI: 10.1002/sml.201001775

independently into each beam, recombined onto BS2, then focused onto the sample inputs using an oil-immersion objective (Olympus UPlanApo, 100×, numerical aperture = 1.35). The phase of the beam in *EXT 1* was controlled with respect to *EXT 2* by a Babinet compensator (BC). A scanning electron microscopy (SEM) image of the “y” structure is shown in Figure 1b. The SPPs launched at input 1 propagated along the short wire and were then coupled into the main wire via the junction (Figure 1b). The emission from the modulator output was recorded by a thermoelectric (TE)-cooled 1392 × 1040 charge-coupled device (CCD) detector. The polarization and power at the two inputs were controlled by half-wave plates and attenuators in each input beam. The polarization angle at each input was rotated to ensure maximal emission from the output, as illustrated by the arrows in Figure 1c. Figure 1c and d shows the modulator excited simultaneously at both inputs. For the same incident polarization at each input, the emission intensity at the output can be controlled, depending on the relative phase of the two input beams. The emission intensity can be expressed as the coherent superposition of  $|E_1 e^{-i(\omega + \Delta_1)} + E_2 e^{-i(\omega + \Delta_2)}|^2$ , where  $E_1$  and  $E_2$  are the electric fields of the emission resulting from the SPPs launched at inputs 1 and 2, respectively,  $\omega$  is the frequency of the free-space emission observed at the output, and  $\Delta_1$  and  $\Delta_2$  are the phases of each of the SPPs at the output. By tuning the BC, the phase difference between the two SPPs,  $\Delta = \Delta_1 - \Delta_2$  was varied.

Figure 2a shows the output emission intensity from the modulator as a function of phase change  $\Delta$  between the two inputs. Individual excitation at inputs 1 or 2, with incident powers of 0.8 and 0.4  $\mu\text{W}$ , respectively, results in emission at the output with similar intensities (triangles and circles), that is,  $I_1 \approx |E_1|^2$ ,  $I_2 \approx |E_2|^2$ . For simultaneous excitation at both inputs 1 and 2, the intensity exhibits a distinct, phase-dependent interference, which is proportional to  $|E_1|^2 + |E_2|^2 + 2E_1 E_2 \cos(\Delta)$ . When  $\Delta = 0^\circ$ , corresponding to the image shown in Figure 1c, constructive interference between the SPPs from the two inputs results in  $I_{12} \approx 4|E_1|^2$ . For a  $\Delta = 180^\circ$  phase shift between the two inputs, corresponding to

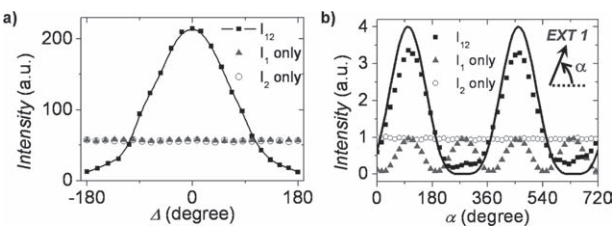


**Figure 2.** a) Emission as a function of the phase difference. Squares: emission intensity from 3 when the inputs 1 and 2 are simultaneously excited. Triangles: only input 1 is excited. Circles: only input 2 is excited. The laser powers at inputs 1 and 2 are 0.8 and 0.4 mW, respectively. The polarization of both inputs 1 and 2 are the same as in Figure 1c. b) Emission as a function of incident polarization angle. Squares: both inputs 1 and 2 are excited simultaneously. Triangles: only input 1 is excited. Circles: only input 2 is excited. The incident polarization angle is rotated anticlockwise. The incident polarization at 2 is parallel to the wire. The phase difference  $\Delta$  when  $\alpha = 101^\circ$  is fixed to  $0^\circ$ . All data are normalized by the intensity of  $I_2$ . Curve is from the relation  $|E_2 + E_1 \cos(\alpha - \alpha_0)|^2$ , where  $E_1 = E_2 = 1$ ,  $\alpha_0 = 101^\circ$ , and  $\Delta = 0^\circ$ .

Figure 1d, destructive interference results in an almost complete elimination of emission from the output. By tuning the phase difference, a modulation depth of  $(I_{\max} - I_{\min})/I_{\max} = 0.94$ , corresponding to an intensity ratio of  $I_{\max}/I_{\min} = 18$ , can be obtained. The maximum modulation depth at the output occurs when the intensities of individual SPPs launched from the different input ends are equal to each other at the output terminus. Since the in-coupling efficiencies of light at inputs 1 and 2 are different due to the different geometries of the two input ends, and since the SPPs launched at the different inputs experience different losses before they meet at the main wire, the incident power at the two inputs should be different to achieve the maximum modulation depth. If the same laser power had been used, these differences in in-coupling efficiencies and propagation losses would have resulted in incomplete interference and a smaller modulation depth. The primary reason that the incident power at the branch input (input 1) must be larger than for input 2 is that the plasmons generated at the branch input experience some additional loss when they tunnel from the branch to the main wire at the junction.

The output can also be modulated by changing the polarization angle of one of the input beams (Figure 2b). When input 1 is excited exclusively, the emission from the output oscillates with a period of  $180^\circ$  (triangles). This is due to the strongly polarization-dependent in-coupling efficiency.<sup>[14]</sup> The emission follows the relation  $\cos^2(\alpha - \alpha_0)$ , where  $\alpha$  is the input polarization angle.  $\alpha_0 = 101^\circ$  is the optimal polarization angle for this specific modulator structure. The incident polarization of input 2 is kept at  $90^\circ$  during the rotation of the incident polarization at the input 1. When inputs 1 and 2 are simultaneously excited with the phase difference set to  $\Delta = 0$ , the emission oscillation period as a function of  $\alpha$  is changed to  $360^\circ$  (squares) and the modulation amplitude becomes much stronger than for excitation of only input 1. This phenomenon can also be understood by the interference of two propagating SPPs launched at inputs 1 and 2. As the fundamental plasmon mode in a metallic nanowire ( $m = 0$ ) has a lower propagation loss than its higher-order modes, the output emission is mainly from the  $m = 0$  SPP mode. Hence, the emission intensity can be simply written as  $|E_1 \cos(\alpha - \alpha_0) \cdot e^{i\Delta} + E_2|^2$ . Taking the value  $E_1 = E_2 = 1$ ,  $\alpha_0 = 101^\circ$ , and  $\Delta = 0^\circ$ , the experimental curve can be well reproduced by the black curve shown in Figure 2b, where the small discrepancy may be due to the emission from the  $m = 1$  mode.

To understand the interference of SPPs in nanowires, we performed finite-element method (FEM) simulations of this structure using a commercial electromagnetic analysis package (COMSOL Multiphysics; Figure 3). Our model system is a y-shaped structure consisting of a 5- $\mu\text{m}$  main wire and a 2.5- $\mu\text{m}$  branch wire, each of 200-nm diameter, excited at inputs 1 and 2 with incident polarizations illustrated by the white arrows. The near-field intensity distributions in a plane 5 nm above the modulator are shown in Figure 3a. It is clear that the electric-field intensity along the main wire becomes strong (top,  $\Delta = 0^\circ$ ) or weak (bottom,  $\Delta = 180^\circ$ ) depending on the phase difference between these two excitations. This simulation confirms that the observed modulation of the emission is due to the interference of SPPs in the nanowire, rather

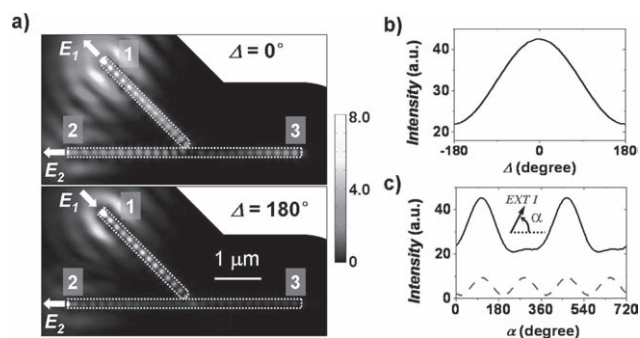


**Figure 3.** FEM simulations of phase and polarization modulation in silver nanobranched structures. a) Local electric-field intensity distribution of a nanobranched of 200-nm diameter excited simultaneously at inputs 1 and 2. The polarization at each input is indicated by the white arrows. The phase difference of SPPs from inputs 1 and 2 is  $\Delta = 0^\circ$  (top) and  $180^\circ$  (bottom). b) Emission intensity at output 3 as a function of phase difference  $\Delta$ . The incident polarizations are the same as that in (a). c) Emission intensity modulated by the incident polarization angle at the terminal 1. Solid curve: both inputs 1 and 2 are excited. Dashed curve: only input 1 is excited. The incident polarization angle is rotated anticlockwise.

than an interference of fields at the detector. The dependence of the intensity at the output on the phase difference at the two inputs, and on the polarization angle at one of the inputs, as shown in the measurements in Figure 2, is reproduced qualitatively by the simulation result (Figure 3b).

A plasmonic modulator can also be realized in a nanowire–nanoparticle system, as illustrated in Figure 4a. Here, nanowire SPPs are launched by optical excitations at opposite ends of the nanowire (1, 2). A nanoparticle adjacent to the nanowire at an arbitrary point along its length can serve as the modulator output site (3).

As shown in Figure 4b, the SPPs launched at the nanowire end points result in bright emission out-coupled at the position of the nanoparticle.<sup>[14]</sup> By tuning the phase difference at the two inputs, the output emission intensity can be modulated in this geometry (squares in Figure 4c). The ratio between the constructive and destructive interference in this structure is  $\approx 2.5$ . Emission from the nanoparticle output site for individual excitation of each wire end is independent of phase modulation (triangles and circles), confirming that the modulation observed in Figure 4b is due to SPP interference. Another distinct and unusual geometry for the nanowire-based modulator is shown in Figure 4d: a nanowire with two adjacent nanoparticle outputs, A and B, with the particle separation  $\approx 1.3 \mu\text{m}$ . The emission from both nanoparticle outputs is shown as a function of the relative phase of the input beams,  $\Delta$  (Figure 4f). The measured ratios between constructive and destructive interference are  $\approx 4$  and  $3.4$  at output sites A and B, respectively. Differences in incident power at the two inputs, differences in propagation distances to the two output sites, and likely variations in out-coupling efficiencies for the output sites all contribute to this observed difference in modulation depth between A and B. Within the resolution of the phase compensator  $\approx \pi/25$ , the emission from these two nanoparticle output sites are modulated synchronously. This nanowire–multiple-nanoparticle structure could thus be used as a multiple-output plasmonic modulator.

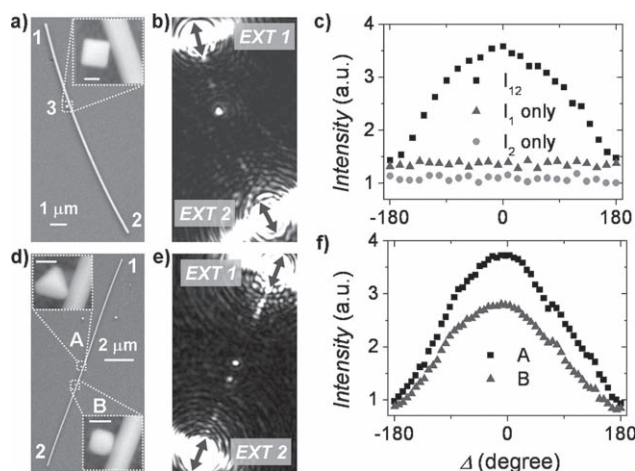


**Figure 4.** Plasmon modulation in a nanowire–nanoparticle system. a) SEM image of a nanowire with an adjacent nanoparticle. The scale bar in the inset showing the detail of the wire–particle junction is 100 nm. b) Optical image of simultaneous excitations of inputs 1 and 2. c) Emission intensity from the nanoparticle in (a) as a function of the phase difference at the two inputs. Squares: emission intensity from nanoparticle for simultaneous excitation of inputs 1 and 2. Triangles: only input 1 is excited. Circles: only input 2 is excited. The laser powers at inputs 1 and 2 are 0.3 and 0.9 mW, respectively. d) SEM image of a nanowire modulator with two adjacent nanoparticles serving as output sites. The scale bars in both insets showing the details of the wire–particle junction are 100 nm. e) Optical image of the wire for simultaneous excitations of inputs 1 and 2. Arrows in (b) and (e) show the incident polarization angles at each input. f) Emission intensity from particle A (squares) and B (triangles) as a function of the phase difference,  $\Delta$ , for simultaneous excitation. The laser powers at inputs 1 and 2 are 3.8 and 0.8 mW, respectively.

In conclusion, we have shown that a silver-nanowire branched structure with two inputs can serve as a plasmonic modulator, controlled by the relative phase or polarization of the input light beams. We have investigated this coherent interference both in nanobranched “y” structures and in nanowire–nanoparticle structures, where nanoparticles serve as output sites. The modulation depth can be greater than 90%, depending on the specific geometry of the structure. These findings show that nanowire-based geometries can serve as ultracompact optical components for controllably imparting information onto both surface-bound and emitted free-space optical signals.

## Experimental Section

Crystalline Ag nanowires were synthesized using a wet chemical method. First, 3 mL ethylene glycol (EG) solution ( $0.1 \text{ mol L}^{-1}$ ) of  $\text{AgNO}_3$  was added to 3 mL EG solution ( $0.6 \text{ mol L}^{-1}$ ) of poly(vinyl pyrrolidone) (PVP K30). After 10 min, the 6 mL solution was injected dropwise into 5 mL EG at  $160^\circ\text{C}$  during a 6-min time period. After injection, the solution was heated at  $160^\circ\text{C}$  for 1 h. Magnetic stirring was applied continuously throughout the entire process. Finally, the whole solution was cooled, washed via centrifugation once in acetone to remove the EG, then washed twice in ethanol to remove the residual PVP. Ag nanowires in ethanol were then deposited on the substrate with marked grids, then

dried. Self-assembled nanobranches were found by scanning the sample surface with an optical microscope (Olympus BX 51). SEM images of the structures identified for study were obtained using a Hitachi S-4800 SEM system. Finally, optical measurements were performed under an oil-immersion objective (UPlanApo, 100 $\times$ , numerical aperture = 1.35).

FEM simulations were performed assuming a homogeneous dielectric background with dielectric constant  $\epsilon = 2.25$ . Scattering boundary conditions were adapted to truncate the boundaries. The permittivity for Ag at the vacuum wavelength of 632.8 nm is taken as  $\epsilon_{\text{Ag}} = -18.36 + 0.4786i$ . The emission power at the output terminal was integrated after a near-to-far-field transformation at the local position. In our simulations, the ratio of the incident electromagnetic fields at terminals 1 and 2 was 2:1.

## Acknowledgements

This work was supported by MOST Grants (No. 2009CB930700), NSFC Grants (Nos. 10904171, 10625418, 10874233 and 11004237), the "Bairen Project" and the "Visiting Professorship for Senior International Scientists" of CAS, and the Robert A. Welch Foundation under grants C-1220 (NJH) and C-1222 (PN). We thank Prof. Baoli Liu for experimental support.

- [1] R. Zia, J. A. Schuller, A. Chandran, M. L. Brongersma, *Mater. Today* **2006**, *9*, 20–27.
- [2] E. Ozbay, *Science* **2006**, *311*, 189–193.
- [3] R. Kirchain, L. Kimerling, *Nat. Photonics* **2007**, *1*, 303–305.
- [4] F. J. García de Abajo, J. Cordon, M. Corso, F. Schiller, J. E. Ortega, *Nanoscale* **2010**, *2*, 717–721.
- [5] Z. Ma, X. I. Zhang, X. Guo, Q. Yang, Y. G. Ma, L. M. Tong, *Appl. Phys. Lett.* **2010**, *96*.
- [6] S. H. Guo, D. G. Britti, J. J. Heetderks, H. C. Kan, R. J. Phaneuf, *Nano Lett.* **2009**, *9*, 2666–2670.
- [7] D. A. Clayton, D. M. Benoist, Y. Zhu, S. L. Pan, *ACS Nano* **2010**, *4*, 2363–2373.
- [8] L. M. Tong, V. D. Miljkovic, M. Kall, *Nano Lett.* **2010**, *10*, 268–273.
- [9] H. Staleva, G. V. Hartland, *Adv. Funct. Mater.* **2008**, *18*, 3809–3817.
- [10] N. Lawrence, L. Dal Negro, *Opt. Express* **2010**, *18*, 16120–16132.
- [11] T. Vo-Dinh, A. Dhawan, S. J. Norton, C. G. Khoury, H. N. Wang, V. Misra, M. D. Gerhold, *J. Phys. Chem. C* **2010**, *114*, 7480–7488.
- [12] J. M. Baik, S. J. Lee, M. Moskovits, *Nano Lett.* **2009**, *9*, 672–676.
- [13] H. Ditzbacher, A. Hohenau, D. Wagner, U. Kreibig, M. Rogers, F. Hofer, F. R. Aussenegg, J. R. Krenn, *Phys. Rev. Lett.* **2005**, *95*, 257403.
- [14] M. W. Knight, N. K. Grady, R. Bardhan, F. Hao, P. Nordlander, N. J. Halas, *Nano Lett.* **2007**, *7*, 2346–2350.
- [15] Z. P. Li, F. Hao, Y. Z. Huang, Y. R. Fang, P. Nordlander, H. X. Xu, *Nano Lett.* **2009**, *9*, 4383–4386.
- [16] Z. P. Li, K. Bao, Y. R. Fang, Y. Z. Huang, P. Nordlander, H. X. Xu, *Nano Lett.* **2010**, *10*, 1831–1835.
- [17] P. Tuchscherer, C. Rewitz, D. V. Voronine, F. J. García de Abajo, W. Pfeiffer, T. Brixner, *Opt. Express* **2009**, *17*, 14235–14259.
- [18] X. Guo, M. Qiu, J. M. Bao, B. J. Wiley, Q. Yang, X. N. Zhang, Y. G. Ma, H. K. Yu, L. M. Tong, *Nano Lett.* **2009**, *9*, 4515–4519.
- [19] Y. R. Fang, Z. P. Li, Y. Z. Huang, S. P. Zhang, P. Nordlander, N. J. Halas, H. X. Xu, *Nano Lett.* **2010**, *10*, 1950–1954.
- [20] P. H. C. Camargo, C. M. Cobley, M. Rycenga, Y. N. Xia, *Nanotechnology* **2009**, *20*.
- [21] T. Kang, S. M. Yoo, I. Yoon, S. Y. Lee, B. Kim, *Nano Lett.* **2010**, *10*, 1189–1193.
- [22] T. Shegai, Z. P. Li, T. Dadoosh, Z. Zhang, H. X. Xu, G. Haran, *Proc. Natl. Acad. Sci. USA* **2008**, *105*, 16448–16453.
- [23] Z. P. Li, T. Shegai, G. Haran, H. X. Xu, *ACS Nano* **2009**, *3*, 637–642.
- [24] D. Pacifici, H. J. Lezec, H. A. Atwater, *Nat. Photonics* **2007**, *1*, 402–406.
- [25] J. A. Dionne, K. Diest, L. A. Sweatlock, H. A. Atwater, *Nano Lett.* **2009**, *9*, 897–902.
- [26] W. S. Cai, J. S. White, M. L. Brongersma, *Nano Lett.* **2009**, *9*, 4403–4411.
- [27] R. X. Yan, P. Pausauskie, J. X. Huang, P. D. Yang, *Proc. Natl. Acad. Sci. USA* **2009**, *106*, 21045–21050.
- [28] Y. G. Sun, B. Mayers, T. Herricks, Y. N. Xia, *Nano Lett.* **2003**, *3*, 955–960.

Received: October 8, 2010  
 Revised: November 26, 2010  
 Published online: January 31, 2011